Dietary lipids, not ketone body metabolites, influence intestinal tumorigenesis in a ketogenic diet

Jessica E.S. Shay[1,2,#], Fangtao Chi[1,#], Constantine N. Tzouanas[1,3-5], Johanna Ten Hoeve[6], Kevin J. Williams[7], Tolga Sever[1], Isabela Fuentes[8,9], Ömer H. Yilmaz[1,2-4,9-11]

[1]David H. Koch Institute for Integrative Cancer Research, MIT, Cambridge, MA 02139, USA

[2]Gastrointestinal Unit, Department of Medicine, Massachusetts General Hospital, Harvard Medical School, Boston, MA 02114, USA

[3]Broad Institute of MIT and Harvard, Cambridge, MA 02142, USA

[4]Ragon Institute of MGB and MIT, Cambridge, MA 02142, USA

[5]Institute for Medical Engineering and Science, MIT, Cambridge, MA 02139, USA

[6]UCLA Metabolomics Center, Department of Molecular and Medical Pharmacology, University of California, Los Angeles, Los Angeles, CA 90095, USA

[7]UCLA Lipidomics Core, University of California, Los Angeles, Los Angeles, CA 90095, USA

[8]Cancer Biology Program, Stanford Medicine, Stanford University, Stanford, CA 94305, USA

[9]Department of Biology, Massachusetts Institute of Technology, Cambridge, MA 02139, USA

[10]Department of Pathology, Massachusetts General Hospital and Beth Israel Deaconness Medical Center, Boston, MA 02139, USA

[11]Correspondence to ohyilmaz@mit.edu

[#]These authors contributed equally

Abstract

Diet composition shapes tissue function and disease risk by modulating nutrient availability, metabolic state, and cellular dynamics. In the gastrointestinal tract, obesogenic high-fat diets enhance intestinal stem cell activity and tumorigenesis. However, the impact of ketogenic diets (KD), which contain even higher lipid content but induce ketogenesis, remains poorly understood. This is particularly relevant for patients with familial adenomatous polyposis (FAP), who face a high risk of small intestinal tumours. Here, we combine dietary, genetic, and metabolic manipulations in mouse models of spontaneous intestinal adenoma formation to dissect the role of systemic and epithelial ketogenesis in intestinal cancer. We show that KD accelerates tumour burden and shortens survival, independent of ketone body production. Through genetic manipulation of the ketogenic pathway, we modulate local and systemic ketone body production; however, neither inhibition nor augmentation of the ketogenic enzyme HMGCS2 nor disruption of ketolysis altered tumour progression. In contrast, inhibition of fatty acid oxidation did limit adenomatous formation. These findings reveal that dietary lipid content, through FAO rather than ketone body metabolism, influences intestinal tumorigenesis and highlight the need for nuanced consideration of dietary strategies for cancer prevention in genetically susceptible populations.

42 **Introduction**

43 The influence of diet on tissue homeostasis and cancer risk is a growing concern [1]. The
44 intestinal epithelium is among the most metabolically dynamic tissues in the body, renewing every
45 4-5 days under homeostatic conditions [2]. This regenerative process is orchestrated, in large part,
46 through Lgr5$^+$ intestinal stem cells (ISCs) residing at the base of the small intestinal and colonic
47 crypts [3,4]. Nutrient availability and dietary composition are increasingly recognized as critical
48 modulators of ISC behavior, with growing evidence indicating ISC metabolism influences both cell
49 fate and tumorigenic potential [5,6]. Obesogenic high-fat diets (HFD), emblematic of Western dietary
50 patterns, have been shown to exert pleiotropic and tumorigenic effects throughout the intestinal
51 epithelium [7–10]. HFD promotes the expansion of Lgr5$^+$ ISCs, enhances their clonogenic potential,
52 and increases the likelihood of malignant transformation with additional effects through PPAR-
53 mediated fatty acid oxidation (FAO) and immune evasion [11–16].

54 Dietary interventions like caloric restriction (CR) and short-term 24 hour fasting confer
55 protective effects against age-associated ISC decline and boost stem cell-mediated repair[17–24].
56 With respect to tumorigenicity, we recently found that post-fast refed ISCs and early progenitors
57 initiate greater numbers of tumours in the small intestine and colon upon loss of the *Apc* tumour
58 suppressor gene compared to the ad libitum or fasted states [24]. Ketogenic diets (KDs), while
59 distinct from CR and fasting due to high fat and minimal carbohydrate content, similarly prolong
60 healthspan in mice and demonstrate anti-tumorigenic effects in models of colorectal
61 tumorigenesis; yet, their effects on small intestinal tumorigenesis is less understood [25–27].

62 Nutrient availability, metabolic adaptation, and stem cell function are intimately
63 intertwined, with dietary interventions exerting profound effects on tissue homeostasis,
64 regeneration, and tumorigenesis. The effects of KD on tumorigenesis are somewhat mixed. In an
65 acute myeloid leukemia model, KD accelerated disease progression and reduced survival [28].
66 Similarly, in BRAF V600E mutant melanoma, elevated acetoacetate ketone metabolite levels
67 associated with KD enhanced tumour growth [29]. In a pancreatic cancer allograft model, caloric

68 restriction suppressed tumour growth, whereas KD had no effect [30]. However, KD has
69 demonstrated significant anti-tumorigenic effects in models of colorectal tumorigenesis. Recent
70 work suggests these protective effects are mediated specifically by ketone body metabolites,
71 particularly beta-hydroxybutyrate (BHB), which acts through the hydroxycarboxylic acid receptor
72 2 (HCAR2) to suppress colorectal cancer development. The therapeutic potential of these findings
73 is further highlighted by ongoing clinical investigation of beta-hydroxybutyrate as a
74 chemopreventive agent in Familial Adenomatous Polyposis (FAP) syndrome (NCT06578637), an
75 autosomal dominant hereditary condition characterized by the development of hundreds to
76 thousands of adenomatous polyps in the colon and rectum with near-certain progression to
77 colorectal cancer if left untreated, as well as an increased risk of small intestinal adenomas and
78 cancer [31].

79 3-hydroxy-3-methylglutaryl-CoA synthase 2 (HMGCS2), the rate-limiting mitochondrial
80 enzyme in ketogenesis, catalyzes the condensation of acetyl-CoA and subsequent downstream
81 production of the ketone bodies acetoacetate and beta-hydroxybutyrate (BHB) [32]. While the liver
82 is the principal site of systemic ketone body production, HMGCS2 is also highly expressed in
83 small intestinal ISCs. It is further induced by fasting and ketogenic diets, facilitating the local
84 production of ketone bodies that promote ISC maintenance, proliferation, and regenerative
85 responses through mechanisms such as histone deacetylase inhibition and Notch activation [17,18].
86 However, in the context of FAP, where germline APC mutations drive ISC-mediated adenoma
87 formation, the consequences of enhanced ISC function are not straightforward. This is particularly
88 concerning given that, despite prophylactic colectomy mitigating CRC risk in FAP, extracolonic
89 malignancies have become the leading source of morbidity, with small intestinal, especially
90 duodenal, adenomas and cancer developing in 90% and 10% of patients, respectively [33–37].

91 Understanding the differential impact of ketogenic diets on small intestinal versus colonic
92 tumorigenesis is therefore warranted, especially for FAP patients. While evidence suggests
93 ketone body metabolites like BHB may suppress colorectal cancer development, their role in the

94 small intestine - where FAP patients face the highest cancer risk after prophylactic colectomy -
95 remains undefined. This knowledge gap is particularly significant as dietary interventions,
96 including ketogenic approaches, are increasingly considered as adjunctive strategies in cancer
97 management [38]. Thus, a paradox exists between the lipid-driven enhancement of stemness and
98 the proposed ketone-mediated suppression of tumours [27]. To explore this dichotomy, we combine
99 dietary, genetic, and metabolic manipulations of ketone body metabolite production with inducible
100 Apc loss to determine how modulation of epithelial and systemic ketone body production and
101 utilization impacts tumorigenesis.
102
103 **Results**
104 Ketogenic diet augments ISC function and increases tumorigenesis
105 To study the effects of ketogenesis and ketone body metabolites on the small intestine,
106 we took advantage of a previously defined and characterized purified 80% lard-based ketogenic
107 diet (KD) (**Fig. 1a, Extended Data Fig. 1a, Table 1**). In keeping with prior findings, mice on a KD
108 exhibited modest weight changes (**Fig. 1b, Extended Data Fig. 1b, c**) and significantly higher
109 circulating ketones compared to mice on a purified control diet (CD) (**Fig. 1c**). Although no
110 significant changes in glucose were noted (**Fig. 1d**), KD mice had decreased circulating insulin
111 when compared to CD mice (**Fig. 1e**). Using the novel Lgr5-2A-EGFP-2A-CreERT2 reporter
112 mouse with GFP expression in all intestinal crypt stem cells, we observed an increase in Lgr5
113 GFP^+ crypt base cells and augmented proliferation as seen by $BrdU^+$ staining (**Fig. 1f, g**) [39]. Niche-
114 promoting Paneth cells were decreased (**Extended Data Fig. 1d, e**), indicating that KD ISCs
115 acquire niche independence as observed in an obesogenic HFD model [11]. Supporting this notion
116 further, *in vitro* organoid-forming ability was significantly increased in mice exposed to KD (**Fig.
117 1h, i**), and isolated GFP-expressing stem cells exhibited increased *in vitro* clonogenic growth
118 (**Extended Data Fig. 1f-h**). Lastly, a KD also significantly increased tissue beta-hydroxybutyrate

119 (BHB) levels and the expression of key ketogenic enzymes, such as HMGCS2 (**Fig. 1j, Extended**
120 **Data Fig. 1i**).

121 To directly assess the impact of dietary lipid content and ketogenesis on intestinal
122 tumorigenesis, we utilized Vil-CreERT2 mice that also carry a single Apc floxed allele, allowing
123 for the timed loss of a single copy of Apc upon exposure to tamoxifen. The spontaneous loss of
124 the second Apc allele via loss of heterozygosity leads to adenoma formation. After receiving the
125 tamoxifen injection, mice were then placed on either CD or KD for approximately 150 days (**Fig.**
126 **1k**). During this period, a notable increase in premature death was observed, which correlated
127 with the dietary lipid content. KD-exposed mice have shortened survival curves when compared
128 to CD mice (**Fig. 1l**). Tumour burden was increased in KD (**Fig. 1m, n, Extended Data Fig. 1l-**
129 **o**). Regardless of diet, a higher tumour burden exhibited a positive association with serum ketone
130 measurements and a negative association with serum glucose levels measured at the time of
131 tissue collection (**Extended Data Fig. 1j, k**). The pro-tumorigenic effect of KD was even more
132 pronounced at 90 days before the survival curves diverged, indicating that tumour burden likely
133 has a direct effect on mouse survival (**Extended Data Fig. 1l-n**). Hydroxycarboxylic acid receptor
134 2 (HCAR2) has been previously implicated as a BHB receptor that drives the anti-tumorigenic
135 effects of ketone body metabolites in the colon [27]. Interestingly, HCAR2 expression appeared
136 restricted and was absent from early adenomas where nuclear beta-catenin, a hallmark of APC
137 loss and adenoma development, does not co-localize with HCAR2 (**Fig. 1o, Extended Data Fig.**
138 **2a-b**). We sought to examine which cell types expressed Hcar2. In a single-cell RNA sequencing
139 (scRNA-seq) dataset of mouse small intestinal epithelial cells (Aliluev et al; four mice on a high-
140 fat high-sucrose diet, 4205 cells) Hcar2 was detected in 0.2-0.5% of goblet and enteroendocrine
141 cells, respectively, but not in stem cells (**Extended Data Fig. 2c-g**). Hcar2 was also not detected
142 in a separate mouse scRNA-seq intestinal epithelial cell dataset (Mana et al.; eight mice, 62,687
143 cells), and only a single Hcar2 transcript was detected across 15,053 cells in our scRNA-seq of
144 mice on ketogenic vs. control diets (this study). As such, in the small intestine, a ketogenic diet

145 likely exerts tumour-modulating effects in an HCAR2-independent manner in contrast to what has
146 been proposed in the colon.
147
148 Ketone body metabolites are dispensable for the tumorigenic effects of KD
149 To further characterize how KD exposure modulates intestinal epithelial biology, we
150 performed scRNAseq on intestinal epithelial cells isolated from control diet (CD) and KD-treated
151 mice. A total of 15,053 cells were captured and analyzed across conditions (**Fig. 2a, Extended**
152 **Data Fig. 3a**). Among the differentially expressed genes, 3-hydroxymethylglutaryl-CoA synthase
153 2 (*Hmgcs2*) – the rate-limiting enzyme in ketogenesis – was markedly upregulated in ISCs from
154 KD-fed mice (**Fig. 2b, c**). This finding is consistent with prior observations that *Hmgcs2* expression
155 is enriched within Lgr5+ ISCs, with expression declining as cells exit the stem cell compartment
156 and differentiate, and that loss of *Hmgcs2* impairs ISC differentiation and regenerative capacity,
157 effects that can be partially rescued by KD exposure or exogenous beta-hydroxybutyrate (BHB)
158 administration [18].
159 To directly investigate the contribution of epithelial-derived ketone bodies, we generated
160 an inducible intestinal-specific Hmgcs2 knockout model (iKO) by crossing Vil-CreERT2 mice with
161 Hmgcs2$^{fl/fl}$ mice, enabling deletion of Hmgcs2 in all intestinal epithelial cells following tamoxifen
162 administration (**Fig. 2d, e**). KD-induced upregulation of epithelial HMGCS2 was abolished in iKO
163 mice, confirming efficient deletion (**Fig. 2f**). Loss of epithelial HMGCS2 significantly reduced
164 intestinal BHB production without appreciably altering local lipid species, indicating that a
165 substantial fraction of ketone bodies within the intestinal epithelium are produced locally rather
166 than being derived from the circulation and that lipid flux was unlikely to be significantly impacted
167 (**Fig. 2g, Extended Data Fig. 2b**). To complement these findings and examine systemic
168 contributions, we utilized Alb-Cre mice, which constitutively express Cre recombinase under the
169 Albumin promoter, to delete Hmgcs2 specifically in hepatocytes, generating liver-specific
170 knockout (LiKO) mice (**Fig. 2h, i, Extended Data Fig. 3c–f**). LiKO mice exhibited dramatically

171 decreased circulating ketone levels under both fasting and ketogenic dietary conditions (**Fig. 2j**),
172 thereby enabling us to model reductions in systemic ketogenesis.

173 To specifically evaluate the role of local and systemic ketogenesis on tumour development
174 with KD feeding, we crossed both Hmgcs2 iKO and LiKO models into the established $Apc^{fl/wt}$
175 heterozygous background, which sensitizes mice to intestinal adenoma formation following single
176 allele loss of Apc (**Fig. 2k**). As expected, the liver exhibited no significant histopathologic changes
177 following loss of a single Apc allele, likely due to differences in proliferative kinetics between
178 hepatic and intestinal tissues. Based on prior work suggesting a tumor-suppressive effect of BHB,
179 we hypothesized that loss of ketogenesis would exacerbate KD-induced tumour burden.
180 Surprisingly, however, neither intestinal (iKO) nor systemic (LiKO) loss of ketone body production
181 mitigated the pro-tumorigenic effects of a ketogenic diet (**Fig. 2l-m**).

182 Given that ketone body metabolites can also serve as energetic substrates via ketolysis
183 (i.e. a process whereby ketone bodies are converted to acetyl-CoA), we next investigated whether
184 impairing ketone body utilization would affect tumour burden. BHB is oxidized to acetoacetate
185 (AcAc) by the mitochondrial enzyme 3-hydroxybutyrate dehydrogenase 1 (BDH1) and further
186 activated to acetoacetyl-CoA by the enzyme succinyl-CoA:3-ketoacid CoA transferase 1
187 (OXCT1), enabling entry into the tricarboxylic acid (TCA) cycle for energy production. Unlike
188 HMGCS2, which displays a restricted expression profile, both BDH1 and OXCT1 were found to
189 be broadly expressed throughout the intestinal epithelium (**Extended Data Fig. 4a-b**). Loss of
190 BDH1 and OXCT1 allows manipulation of the ketogenic/ketolytic pathways without altering KD-
191 induced HMGCS2 expression (**Extended Data Fig. 4c**). To disrupt ketolytic capacity, we crossed
192 $Bdh1^{fl/fl}$ and $Oxct1^{fl/fl}$ mice into the $Apc^{fl/wt}$ background (**Extended Data Fig. 4d**).

193 Consistent with observations from the HMGCS2 iKO models, loss of BDH1 or OXCT1 did
194 not significantly impact tumour burden (**Extended Data Fig. 4d-f**). These data further
195 demonstrate that neither canonical ketogenesis nor ketolytic pathways in epithelial cells or
196 systemically are required to promote intestinal tumorigenesis in the context of a ketogenic diet.

197 Together, these findings highlight that the pro-tumorigenic effects associated with KD feeding are
198 likely mediated through lipid-driven mechanisms independent of local or systemic ketone body
199 metabolism.
200
201 Induction of ectopic ketogenesis is insufficient to modulate intestinal tumorigenesis
202 A ketogenic diet is characterized by low carbohydrate content and is primarily defined by
203 its high fat composition. To isolate the effects of increased ketone body production from the
204 confounding influence of high dietary lipid intake, we generated a novel Rosa26-LSL-Hmgcs2-
205 2A-mCherry mouse model (hereafter referred to as HMGCS2 iOE), wherein Hmgcs2 expression
206 is placed under Cre recombinase control (**Fig. 3a, Extended Data Fig. 5a**). By crossing these
207 mice to the tamoxifen-inducible Vil-CreERT2 line, we achieved spatial and temporal control of
208 Hmgcs2 expression specifically within the intestinal epithelium, thereby allowing modulation of
209 ketone body production independent of dietary manipulation. Upon tamoxifen
210 induction, HMGCS2 iOE mice exhibited robust and widespread expression of both HMGCS2
211 protein and the linked mCherry reporter in intestinal epithelial cells (**Fig. 3b, Extended Data Fig.
212 5b**).
213 Importantly, ectopic overexpression of Hmgcs2 in the intestinal epithelium led to a
214 significant elevation of local BHB concentrations compared to control animals, despite
215 maintenance on a standard control diet (**Fig. 3c, Extended Data Fig. 5c**). These findings confirm
216 that tissue-specific overexpression of HMGCS2 is sufficient to drive augmented ketone body
217 production *in vivo* without the need for a lipid-enriched or carbohydrate-restricted diet. Thus,
218 the HMGCS2 iOE model enables dissection of the epithelial-intrinsic effects of increased ketone
219 metabolism in the absence of systemic metabolic alterations associated with ketogenic or high-
220 fat diets.
221 To determine whether enhanced epithelial ketone body production influences
222 tumorigenesis, we next assessed spontaneous adenoma formation in Vil-CreERT2; $Apc^{fl/wt}$ mice

223 with or without concurrent Hmgcs2 overexpression, all maintained on a purified control diet.
224 Surprisingly, enforced Hmgcs2 expression, which increased intestinal ketone levels (**Fig. 3c**) did
225 not significantly alter tumour numbers, tumour sizes, or survival compared to wild-type littermates
226 (**Fig. 3d-f**). These data indicate that while epithelial ketone body production can be augmented
227 independently of dietary fat intake, such augmentation alone is insufficient to modify basal
228 intestinal tumorigenesis or clonogenic potential under homeostatic conditions.
229
230 PPAR-mediated long-chain FAO contributes to KD-associated intestinal tumorigenesis
231 To define the impact of a KD on ISC molecular states and metabolism, we conducted
232 transcriptomic analyses of ISCs from mice maintained on either a KD or a control diet (CD). Using
233 CollecTRI, we aimed to identify transcription factors whose genome-wide targets changed in
234 expression with KD. KD exposure significantly increased activation of multiple peroxisome
235 proliferator-activated receptors (PPARs) and PPAR gamma coactivator 1-beta (Ppargc1b) (**Fig.
236 4a**). Additionally, we found that SMADs and SREBF2 were predicted to have increased activity.
237 In contrast, RFXAP/RFANK were predicted to have less activity, suggesting a potential tradeoff
238 with the upregulation of programs involved in lipid metabolism and stem cell maintenance at the
239 expense of MHC II expression. Gene set enrichment analysis (GSEA) revealed robust enrichment
240 of lipid catabolism and fatty acid oxidation (FAO) pathways, including a marked induction of genes
241 involved in mitochondrial long-chain fatty acid transport and β-oxidation with corresponding
242 downregulation in antigen presentation (**Fig. 4b, Extended Data 6a**). We complemented these
243 findings by specifically scoring for markers of PPARs from multiple sources (**Fig. 4c-e**). Among
244 FAO-associated transcripts, carnitine palmitoyltransferase 1A (*Cpt1a*), which catalyzes the rate-
245 limiting step in mitochondrial import of long-chain fatty acids for downstream oxidation, was
246 significantly elevated in KD ISCs compared to CD ISCs (**Fig. 4f**). Immunoblotting confirmed
247 increased CPT1a protein expression in crypt epithelial isolates following KD feeding (**Extended
248 Data Fig. 1i**).

249 To determine the functional relevance of FAO in KD-associated tumorigenesis, we
250 crossed Cpt1a$^{fl/fl}$ mice to Vil-CreERT2;Apc$^{fl/wt}$ mice to generate inducible intestinal-specific Cpt1a
251 knockout (Cpt1a iKO) animals (**Fig. 4g,h)**. Following tamoxifen-induced recombination, cohorts
252 were maintained on KD or CD diets, and spontaneous tumour formation was assessed over time.
253 In the Apc-het background, Cpt1a deletion significantly reduced tumour burden in KD-fed mice
254 compared to WT controls. Quantitative analyses revealed a reduction in the total number of
255 tumours in the Cpt1a iKO cohort in the presence of KD but not CD (**Fig. 4i-j, Extended Data Fig.**
256 **6b-e**). Together, these findings indicate that ketogenic diet-induced PPAR activation enhances
257 ISC function through an FAO-dependent mechanism, with CPT1a acting as a critical metabolic
258 effector. Loss of CPT1a disrupts this pathway, attenuating the KD-associated increase in
259 tumorigenesis. Of note, similar findings are seen when Cpt1a$^{fl/fl}$; Apc$^{fl/wt}$; Lgr5-EGFP-IRES-
260 CreERT2 mice are exposed to a diet with high lipid content [13]. These data highlight mitochondrial
261 FAO rather than ketogenesis or ketone body metabolites as a key node linking dietary lipid
262 exposure, ISC metabolic adaptation, and intestinal cancer risk.
263

264 **Discussion**

265 Here, we demonstrate that a ketogenic diet (KD), despite its physiologic and hormonal
266 profile as distinct from an obesogenic high-fat diet (HFD), shares key tumorigenic features.
267 Through a series of genetic and dietary manipulations, we dissect the contributions of ketogenesis
268 and ketone body metabolism to intestinal tumorigenesis, revealing that dietary lipid and resulting
269 PPAR-mediated FAO, rather than ketone body production, is the principal influencer for KD
270 effects on intestinal tumorigenesis. These findings indicate that while ketone body production is
271 modifiable through diet and genetic perturbation, ketone body metabolites are neither necessary
272 nor sufficient to mediate KD-induced tumorigenesis.

273 In the mouse colon, HMGCS2 expression and ketogenesis are additionally influenced by
274 the resident microbiome (**Extended Data 7a**) [40]. When compared to a purified control diet

275 however, a ketogenic diet increases epithelial beta-hydroxybutyrate (**Extended Data 7b**). This
276 can also be modulated through overexpression of HMGCS2 as with the iOE mouse (**Extended**
277 **Data 7c-d**). The dietary influence of KD on colonic tumour burden in this model is the opposite of
278 the small intestine and yet remains independent of ketone bodies: a KD results in fewer colonic
279 tumours and genetic modulation of epithelial ketones has no discernible anti-tumorigenic effects
280 (**Extended Data 7e-f**). Again, the G-protein coupled receptor HCAR2 has been previously
281 postulated as a key intermediary however, expression appears largely restricted to normal
282 epithelium and is absent from both CD and KD colonic tumours (**Extended Data 7g**). Although
283 beyond the scope of this work, there are numerous changes that occur in the colonic milieu when
284 exposed to high lipid content and these could, in combination, explain some of the observed
285 effects. This work challenges the prevailing notion that ketone bodies are uniformly beneficial or
286 protective against cancer, revealing that in the intestinal epithelium, their effects are diet-
287 modulated yet context-dependent.

288 Importantly, our observations reconcile previous paradoxes in the field. Dietary
289 interventions, such as fasting, caloric restriction, and exogenous ketone supplementation have
290 been associated with enhanced ISC regenerative capacity and reduced tumorigenesis. However,
291 they differ fundamentally from KD in that they lack sustained lipid overload. In a similar manner,
292 the post-fast refeeding exists as a distinct state that can also lead to increased tumour incidence
293 [24]. Thus, the diet composition and systemic metabolic effects must be considered when
294 comparing opposing influences on tumorigenesis such as chronic lipid-induced FAO engagement
295 seen with KD. In conclusion, our findings reveal that a high-fat ketogenic diet influences intestinal
296 tumorigenesis through lipid-driven metabolic reprogramming rather than ketone body signaling,
297 stimulating FAO activation at the earliest stages of tumour initiation. These insights have
298 important implications for dietary interventions in cancer prevention and treatment, particularly in
299 individuals with hereditary cancer predisposition syndromes such as FAP who are prone to small

intestinal tumorigenesis, and highlight the complex interplay between metabolism and oncogenesis in the intestinal epithelium.

Author Contributions

J.E.S.S. and F.C. initiated the project, conceived, designed, performed, and interpreted all experiments and wrote the manuscript with help from O.H.Y.. C.T., J.T.H.S., K.J.W., T.S., and I.F. performed experiments, assisted with data collection and interpretation. J.T.H.S. assisted with intestinal tissue metabolomic analysis. K.J.W. assisted with intestinal tissue lipidomic analysis. All authors assisted in interpreting experiments, writing, and editing the manuscript.

Ethics Declaration

Competing interests: The authors declare no competing interests.

Acknowledgements

We thank the Swanson Biotechnology Center at the Koch Institute, including the Flow Cytometry, Histology, and ES Cell and Transgenics core facilities; the Department of Comparative Medicine for mouse husbandry support; S. Holder and members of the Hope Babette Tang (1983) Histology Facility for substantial histological support; all the members of the Yilmaz laboratory for discussions; K. Kelley for laboratory management; and L. Galoyan for administrative assistance. Ö.H.Y. is supported by the National Institutes of Health (5R01CA245314, R01CA211184, R01CA034992, R01CA257523, R01DK126545, U01CA250554 and U54CA224068); a Pew-Stewart Trust scholar award; the Kathy and Curt Marble cancer research award; a Koch Institute–Dana-Farber/Harvard Cancer Center Bridge project grant; and AFAR. Ö.H.Y. receives support from the MIT Stem Cell Initiative. J.E.S. is supported by an American Gastroenterological Association Research Scholar Award (AGA2025-13-05). F.C. is supported by a Damon Runyon Postdoctoral Fellowship Award (DRG-2463-22).

326

327 **Methods**

328 *Mouse Strains*

329 Mice were under the husbandry care of the Department of Comparative Medicine at the
330 Koch Institute for Integrative Cancer Research at Massachusetts Institute of Technology. All
331 procedures were conducted according to AALAC guidelines and approved by the MIT Committee
332 on Animal Care. Lgr5-2A-EGFP-2A-CreERT2 were created and previously described [39]. Lgr5-
333 eGFP-IRES-CreERT2 (strain name: B6.129P2-Lgr5$^{tm1(cre/ERT2)Cle}$/J; stock number 008875) mice
334 were purchased from Jackson Laboratory. Apc-het mice were created by crossing the previously
335 described Apc^{loxp} exon 14 (Apc$^{fl/fl}$) mice to mice carrying a wild type Apc allele [41]. Villin-CreERT2
336 (Vil-CreERT2) mice were a gift from S. Robine and previously described [42]. Hmgcs2$^{fl/fl}$ were
337 originally generated and described previously [18]. Albumin-Cre mice (strain name B6.Cg-*Speer6-*
338 *ps1*$^{Tg(Alb-cre)21Mgn}$/J; stock number #003574) were purchased from Jackson Laboratory. Bdh1$^{loxp/loxp}$
339 mice were a gift from Daniel Kelly and described previously [43]. Oxct1$^{fl/fl}$ mice were a gift from Peter
340 Crawford and previously described [44]. Rosa26-LSL-Hmgcs2-mCherry mice were created by co-
341 injecting Cas9 mRNA and a donor vector containing "CAG promoter-loxP-3*polyA-loxP-Kozak-
342 mHmgcs2 CDS-2A-mCherry-polyA" cassette into fertilized eggs to generate targeted conditional
343 knockin offspring. Cpt1a$^{fl/fl}$ mice were a gift from Peter Carmeliet and described previously [45]. The
344 following strains were bred in-house: 1) Lgr5-2A-EGFP-2A-CreERT2 , 2) Lgr5-eGFP-IRES-
345 CreERT2, 3) Apc$^{fl/wt}$; Villin-CreERT2, 4) Hmgcs2$^{fl/fl}$; Villin-CreERT2, 5) Hmgcs2$^{fl/fl}$; Albumin-Cre,
346 6) Hmgcs2$^{fl/fl}$; Apc$^{fl/wt}$; Villin-CreERT2, 7) Hmgcs2$^{fl/fl}$; Apc$^{fl/wt}$; Villin-CreERT2; Albumin-Cre, 8)
347 Bdh1$^{fl/fl}$; Apc$^{fl/wt}$; Villin-CreERT2, 9) Oxct1$^{fl/fl}$; Apc$^{fl/wt}$; Villin-CreERT2, 10) Rosa26-LSL-Hmgcs2-
348 mCherry; Villin-CreERT2, 11) Rosa26-LSL-Hmgcs2-mCherry; Apc$^{fl/wt}$; Villin-CreERT2, 12)
349 CPT1a$^{fl/fl}$; Apc$^{fl/wt}$; Villin-CreERT2. All mice were age and sex-matched with both male and female
350 mice used. Food was provided *ad libitum*. Control diet with 10% fat (Research Diet D12450J) and
351 ketogenic diet with 80% fat (Research Diet D06040601) were used throughout experimental

352 conditions with the exception of metabolomic profiling of conventional (CONV) and Hmgcs2 iOE
353 mice where standard chow (LabDiet, 5P76) was used.
354
355 *In vivo treatments*
356 Tamoxifen-induced Cre activation was obtained through intraperitoneal tamoxifen
357 injection suspended in 1 part 100% ethanol to 9 parts sunflower seed oil (Spectrum S1929) at a
358 concentration of 10mg/mL and dosed at 100mg/kg. For tumour studies, mice harboring
359 conditional alleles plus $Apc^{fl/wt}$ were administered tamoxifen two times within one week. For
360 additional non-tumor studies, mice were administered tamoxifen three times within one week.
361 BrdU (sigma Aldrich, 19-160) was prepared at 10mg/mL in PBS and injected at 100mg/kg 4 hours
362 prior to tissue collection.
363
364 *Tumor analysis*
365 Intestine was dissected out and flushed with 4°C PBS before being placed in histology
366 cassettes and fixed overnight in 10% formalin. Tissue was then transferred to 70% ethanol before
367 additional dehydration steps and embedding. 4-5μm sections were stained with hematoxylin and
368 eosin and scanned in at 20x magnification using Leica Aperio Slide Scanner. SVS files were then
369 analyzed using QuPath in a blinded manner.
370
371 *Serum measurements*
372 Circulating glucose and ketones were measured by collecting tail vein blood and using
373 FreeStyle Precision Neo System Kit with Blood Glucose and Ketone Test Strips (Abbott). Plasma
374 was collected via cardiac puncture into capillary blood collection vial (Microvette 20.1292.100)
375 before separation via centrifugation. Circulating insulin was then quantified via wide-range ultra
376 sensitive ELISA (Crystal Chem #90080).

377

378 *Tissue metabolic profiling*

379 For metabolomics, intestine tissue was quickly dissected out, washed twice with 150mM
380 Ammonium acetate, and snap-frozen into liquid nitrogen. The snap-frozen tissue was then
381 homogenized into powder using mortar-pestle in liquid nitrogen. About 50mg of the tissue powder
382 was used for metabolites extraction in 80% MeOH with OMNI bead homogenizer. The
383 tissue/80%MeOH mixture was incubated for 24 hours at −80°C and then centrifuged (16,000 g)
384 for 20 minutes at 4°C. The MeOH supernatants were transferred into new tubes and placed on
385 ice. The sample pellets were resuspended in 500µl 0.2M NaOH, heated at 95°C for 10 minutes,
386 and the protein concentration was measured by BCA assay using 1:10 dilution. Finally, the 500
387 µg protein equivalent of MeOH supernatants were dried using multivap nitrogen evaporator. Dried
388 metabolites were resuspended in 50% ACN:water at 50 mg tissue extract/ml. 5µl was loaded onto
389 a Luna NH2 3um 100A (150 × 2.0 mm) column (Phenomenex) using a Vanquish Flex UPLC
390 (Thermo Scientific). The chromatographic separation was performed with mobile phases A (5 mM
391 NH4AcO pH 9.9) and B (ACN) at a flow rate of 200 µl/min. A linear gradient from 15% A to 95%
392 A over 18 min was followed by 7 min isocratic flow at 95% A and reequilibration to 15% A.
393 Metabolites were detected with a Thermo Scientific Q Exactive mass spectrometer run with
394 polarity switching in full scan mode using a range of 70-975 m/z and 70.000 resolution. Maven (v
395 8.1.27.11) was used to quantify the targeted polar metabolites by AreaTop, using expected
396 retention time and accurate mass measurements (< 5 ppm) for identification. Data analysis,
397 including principal component analysis and heat map generation was performed using in-house
398 R scripts.

399 For lipidomics, isolated intestine tissue was snap frozen in liquid nitrogen. 50mg of
400 homogenized tissue was then sent to UCLA Lipidomics in 2mL homogenizer tubes pre-loaded
401 with (6) 2.8mm ceramic beads (Omni #19-628). 750ul PBS was added to the tube and
402 homogenized in the Omni Bead Ruptor Elite (3 cycles of 10 seconds at 5 m/s with a 10 second

403 dwell time). Homogenate containing 1-8mg of original tissue was transferred to a glass tube for
404 extraction. A modified Bligh and Dyer extraction was carried out on all samples [46]. Prior to
405 biphasic extraction, a standard mixture of 75 lipid standards based on Avanti Ultimate Splash
406 ONE mix was used (Avanti 330820, 861809, 330729, 330727, 791642, 330726). Following two
407 successive extractions, pooled organic layers were dried down in a Thermo SpeedVac
408 SPD300DDA using ramp setting 4 at 35 degrees C for 45 minutes with a total run time of 90
409 minutes. Lipid samples were resuspended in 1:1 methanol/dichloromethane with 10mM
410 Ammonium Acetate and transferred to robovials (Thermo 10800107) for analysis. Samples were
411 analyzed on the Sciex 6500+ with DMS device with an expanded targeted acquisition list
412 consisting of 1450 lipid species across 17 subclasses. Differential Mobility Device was tuned with
413 EquiSPLASH LIPIDOMIX (Avanti 330731). Data analysis performed on an in-house data analysis
414 platform comparable to the Lipidyzer Workflow Manager with instrument method including
415 settings, tuning protocol, and MRM list as described [47]. Quantitative values were normalized to
416 mg of tissue.
417
418 *Crypt and ISC isolation and culturing*
419 Intestine was removed and flushed with 4°C PBS (no calcium, no magnesium), opened
420 laterally and gently cleaned and cut into sections before rinsing and incubation at 4°C in 10mM
421 EDTA for 40 minutes. Crypts were then mechanically separated by shaking and filtering through
422 70um mesh to remove villi and tissue fragments. Isolated crypts and flow isolated ISCs were
423 counted and embedded in Matrigel (Corning 356231) as previously described [13].
424
425 *Flow cytometry*
426 Following crypt isolation, crypt suspensions were pelleted (100g, 5 min, 4°C) and
427 supernatant was discarded. Crypts were resuspended in TrypLE (GIBCO, no phenol red,

428 1264039) and dissociated into individual cells by warming crypts in a 32°C water bath for 60
429 seconds. Dissociated single cells were incubated with the following antibodies for flow cytometry
430 analysis: CD45-PE (eBioscience, 12-0451-83), CD31-PE (BioLegend, 102514), Ter-119PE
431 (Biolegend, 116208), CD24-Pacific Blue (Biolegend, 101820), CD117-APC/Cy7 (Biolegend,
432 105826), and EpCAM-APC (eBioscience, 17-5791-82). 7AAD (Invitrogen, A1310) was used as a
433 viability dye to exclude dead cells from analysis. Intestinal stem cells (ISCs) and progenitors were
434 isolated as Lrg5-eGFP^{hi}EpCAM^{+}CD24$^{low/-}$CD31^{-}Ter119^{-}CD45^{-}7AAD^{-} and Lrg5-
435 eGFP^{low}EpCAM^{+}CD24$^{low/-}$CD31^{-}Ter119^{-}CD45^{-}7AAD^{-}, respectively. Cells were sorted using a BD
436 FACS II SORP cell sorter.
437
438 *scRNA-seq processing*
439 Cells were sorted with the same parameters as described above for flow-cytometry into
440 an Eppendorf tube containing 50ml of 0.4% BSA-PBS and stored on ice until proceeding to the
441 Chromium Single Cell Platform. Single cells were processed through the Chromium Single Cell
442 Platform using the Chromium Single Cell 3' Library, Gel Bead and Chip Kits (10X Genomics,
443 Pleasanton, CA), following the manufacturer's protocol. Briefly, an input of 7,000 cells was added
444 to each channel of a chip with a recovery rate of 1,500-2,500 cells. The cells were then partitioned
445 into Gel Beads in Emulsion (GEMs) in the Chromium instrument, where cell lysis and barcoded
446 reverse transcription of RNA occurred, followed by amplification, tagmentation and 50 adaptor
447 attachment. Libraries were sequenced on an Illumina NextSeq 500.
448 The CellRanger pipeline was used to align sequencing reads to the mm10 genome
449 according to manufacturer recommendations. Cells were pre-processed to remove cells with
450 fewer than 1,750 UMIs detected (likely corresponding to detection of ambient RNA or low-quality
451 cells) or more than 75,000 UMIs (likely corresponding to doublets). Data was then analyzed using
452 Seurat in R with normalization implemented via SCTransform's regularized negative binomial
453 regression. For downstream visualization and clustering, principal component analysis was

454 performed on the highly variable genes returned from SCTransform, with the number of principal
455 components made by examining the elbow plot of variance explained by each principal
456 component (results robust against alternate choices of QC and visualization parameters). UMAP
457 visualization was implemented using the ''uwot'' R package. Stem cells were identified using a
458 module score of core intestinal stem cell genes calculated with Seurat's ''AddModuleScore''
459 function (*Lgr5*, *Axin2*, *Olfm4*, *Lrig1*, *Fzd7*), as previously described [13]. Stem cells were additionally
460 scored for modules of PPAR target genes (*Hmgcs2*, *Angptl4*, *Pdk4*, *Acsl3*, *Me1*, *Acot1*, *Reg3g*,
461 *Plin2*), fatty acid oxidation-related genes regulated by PPAR (*Cpt1a*, *Acadvl*, *Cact*, *Acadl*, *Hadha*,
462 *Hadhb*, *Eci2*), and the WikiPathways PPAR Signaling gene set, as previously described [13]. GSEA
463 was run through the fgsea package [48] . CollecTRI was run through the decoupleR package, and
464 effect sizes were calculated as signed Cohen's D effect sizes [49]. Statistical significance was
465 calculated for differential gene expression, differential module scores, and differential
466 transcription factor activities using the non-parametric Mann-Whitney test and adjusted for
467 multiple hypothesis testing using the Benjamini-Hochberg correction.
468
469 *Immunohistochemistry and Immunofluorescence*
470 Tissue was fixed in 10% normal buffered formalin prior to paraffin-embedding. 4-5μm micron
471 sections underwent deparaffinization and rehydration prior to antigen retrieval using Borg
472 Decloacker RTU solution (Biocare Medical, BD1000G1) and a pressurized Decloaking Chamber
473 (Biocare Medical, NxGen). Antibodies and respective dilutions used for immunohistochemistry
474 are as follows: goat polyclonal anti-GFP (1:1000, Abcam, ab6673), rat anti-BrdU (1:2000, Abcam,
475 6326), rabbit polyclonal anti-lysozyme (1:2000, ThermoFisher, RB-372-A1), rabbit monoclonal
476 anti-HMGCS2 (1:2000, Abcam, ab137043), rabbit polyclonal anti-OXCT1 (1:1000, Sigma-Aldrich,
477 HPA012047), rabbit polyclonal anti-BDH1 (1:500, Proteintech, 15417-1-AP), with dilutions
478 performed in Signalstain Antibody Diluent (Cell Signaling Technology, #8112). Biotin conjugated
479 secondary donkey anti-rabbit antibodies (1:500, Jackson ImmunoResearch) were used prior to

480 Vectastain Elite ABC immunoperoxidase detection kit (Vector Laboratories, PK6100).
481 Visualization was performed using Signalstain DAB substrate kit (Cell Signaling Technology,
482 #8049). Counterstaining was performed with 50% Gill No. 1 hematoxylin solution (Sigma-Aldrich,
483 GHS116). Images were acquired using an Olympus BX43 microscope with 4x and 10x objectives
484 (Olympus UPlanSApo). The following primary antibodies were used for immunofluorescence:
485 rabbit polyclonal anti-HCAR2 (1:200, ThermoFisher, PA5-50671) and mouse monoclonal anti-
486 beta-catenin (1:200, BD Biosciences, 610164). Alexa Fluor secondary antibodies, anti-mouse 488
487 and anti-rabbit 568 were use for visualization. Tissue was mounted using Invitrogen Prolong Gold
488 mounting medium containing DAPI. Images were acquired using an Olympus FV1200 Laser
489 Scanning Confocal Microscope.
490
491 *Immunoblotting*
492 Snap frozen tissue was crushed into a fine powder before elution with RIPA buffer and tissue
493 homogenizer. Isolated crypts were resuspended in RIPA buffer for lysis. In both cases, after
494 centrifuging at 10,000 rpm for 15 minutes at 4°C, the resulting supernatant was quantified using
495 the Pierce BCA protein assay kit (23225, Thermo Fisher Scientific) then suspended in Laemmli
496 SDS sample buffer (J61337-AC, VWR) at a concentration of 2ug/ul and boiled for 5 minutes at
497 95°C. 20ug protein per sample was separated on 4-12% gradient gel (NuPAGE Bis-Tris Mini
498 Protein, Invitrogen, NP0336BOX) and transferred onto a 0.45 micron PVDF membrane
499 (Immobilon-P transfer, Millipore, ipvh00010) and analyzed by immunoblotting using rabbit
500 monoclonal anti-HMGCS2 (1:1000, Abcam, ab137043), mouse monoclonal anti-CPT1a (1:1000,
501 Abcam, ab128568), rabbit polyclonal anti-BDH1 (1:1000, Proteintech, 15417-1-AP), rabbit
502 polyclonal anti-OXCT1 (1:1000, Sigma-Aldrich, HPA012047), rabbit monoclonal anti-vinculin
503 (1:1000, Cell Signaling Technology, #13901) followed by horseradish peroxidase (HRP)-
504 conjugated IgG secondary antibodies (1:3000, Cell Signaling Technology, #7076, #7074) and

505 ECL detection kit (ECL K-12045-D20 and Sirius K-12043-D20, Advansta). Quantitative
506 chemiluminescent imaging was performed using the ImageQuant LAS 4000 (GE Healthcare).
507
508 *Statistics and Reproducibility*
509 Unless otherwise specified in the main text or figure legends, all experiments reported in this study
510 were repeated at least three independent times. Unless otherwise specified in the main text or
511 figure legend, all sample numbers (n) represent biological replicates. No sample or animals were
512 excluded from analysis, and sample size estimates were not used. Studies were not conducted
513 blind with the exception of all histological analyses. Age-matched and sex-matched mice were
514 randomly assigned to groups. All values are presented as mean ± s.d. Unless otherwise specified
515 in the figure legend, intergroup comparison was performed using unpaired two-tailed t-tests. In
516 the case of more than two comparison groups, ANOVA with Tukey's was performed. Statistical
517 analysis was performed using GraphPad Prism 10. Statistical details can be found in the figure
518 legends.
519
520 *Data availability*
521 Datasets generated in this study will be made publicly available upon publication.
522

References

1. Willett, W. C., Stampfer, M. J., Colditz, G. A., Rosner, B. A. & Speizer, F. E. Relation of Meat, Fat, and Fiber Intake to the Risk of Colon Cancer in a Prospective Study among Women. *New England Journal of Medicine* **323**, 1664–1672 (1990).

2. Haber, A. L. *et al.* A single-cell survey of the small intestinal epithelium. *Nature* **551**, 333–339 (2017).

3. Barker, N. *et al.* Identification of stem cells in small intestine and colon by marker gene Lgr5. *Nature* **449**, 1003–1007 (2007).

4. Sato, T. *et al.* Single Lgr5 stem cells build crypt-villus structures in vitro without a mesenchymal niche. *Nature* **459**, 262–5 (2009).

5. Shay, J. E. S. & Yilmaz, Ö. H. Dietary and metabolic effects on intestinal stem cells in health and disease. *Nature Reviews Gastroenterology & Hepatology* (2024) doi:10.1038/s41575-024-00980-7.

6. Lien, E. C. & Heiden, M. G. V. A framework for examining how diet impacts tumour metabolism. *Nature Reviews Cancer* **19**, 651–661 (2019).

7. Mehta, R. S. *et al.* Dietary Patterns and Risk of Colorectal Cancer: Analysis by Tumor Location and Molecular Subtypes. *Gastroenterology* **152**, 1944-1953.e1 (2017).

8. Zaborowski, A. M. *et al.* Characteristics of Early-Onset vs Late-Onset Colorectal Cancer. *JAMA Surgery* **156**, 865 (2021).

9. Collaborators, undefined T. G. 2015 O. Health Effects of Overweight and Obesity in 195 Countries over 25 Years. *New England Journal of Medicine* **377**, 13–27 (2017).

10. Ng, M. *et al.* Global, regional, and national prevalence of overweight and obesity in children and adults during 1980–2013: a systematic analysis for the Global Burden of Disease Study 2013. *The Lancet* **384**, 766–781 (2014).

11. Beyaz, S. *et al.* High-fat diet enhances stemness and tumorigenicity of intestinal progenitors. *Nature* **531**, 53–58 (2016).

12. Beyaz, S. *et al.* Dietary suppression of MHC class II expression in intestinal epithelial cells enhances intestinal tumorigenesis. *Cell Stem Cell* **28**, 1922-1935.e5 (2021).

13. Mana, M. D. *et al.* High-fat diet-activated fatty acid oxidation mediates intestinal stemness and tumorigenicity. *Cell Reports* **35**, 109212 (2021).

14. DeClercq, V., McMurray, D. N. & Chapkin, R. S. Obesity promotes colonic stem cell expansion during cancer initiation. *Cancer Letters* **369**, 336–343 (2015).

556 15. Wasan, H. S., Novelli, M., Bee, J. & Bodmer, W. F. Dietary fat influences on polyp
557 phenotype in multiple intestinal neoplasia mice. *Proceedings of the National Academy of*
558 *Sciences of the United States of America* **94**, 3308–3313 (1997).

559 16. Newmark, H. L. *et al.* A Western-style diet induces benign and malignant neoplasms in the
560 colon of normal C57Bl/6 mice. *Carcinogenesis* **22**, 1871–1875 (2001).

561 17. Mihaylova, M. M. *et al.* Fasting Activates Fatty Acid Oxidation to Enhance Intestinal Stem
562 Cell Function during Homeostasis and Aging. *Cell Stem Cell* **22**, 769-778.e4 (2018).

563 18. Cheng, C.-W. *et al.* Ketone Body Signaling Mediates Intestinal Stem Cell Homeostasis and
564 Adaptation to Diet. *Cell* **178**, 1115-1131.e15 (2019).

565 19. Pak, H. H. *et al.* Fasting drives the metabolic, molecular and geroprotective effects of a
566 calorie-restricted diet in mice. *Nature Metabolism* **3**, 1327–1341 (2021).

567 20. Bruens, L. *et al.* Calorie Restriction Increases the Number of Competing Stem Cells and
568 Decreases Mutation Retention in the Intestine. *Cell Reports* **32**, 107937 (2020).

569 21. Mai, V. *et al.* Calorie restriction and diet composition modulate spontaneous intestinal
570 tumorigenesis in Apc(Min) mice through different mechanisms. *Cancer Res.* **63**, 1752–5 (2003).

571 22. Mitchell, S. J. *et al.* Daily Fasting Improves Health and Survival in Male Mice Independent of
572 Diet Composition and Calories. *Cell Metabolism* **29**, 221-228.e3 (2019).

573 23. Yilmaz, Ö. H. *et al.* MTORC1 in the Paneth cell niche couples intestinal stem-cell function to
574 calorie intake. *Nature* **486**, 490–495 (2012).

575 24. Imada, S. *et al.* Short-term post-fast refeeding enhances intestinal stemness via polyamines.
576 *Nature* **633**, 895–904 (2024).

577 25. Roberts, M. N. *et al.* Short Article A Ketogenic Diet Extends Longevity and Healthspan in
578 Adult Mice Short Article A Ketogenic Diet Extends Longevity and Healthspan in Adult Mice. *Cell*
579 *Metabolism* **26**, 539-546.e5 (2017).

580 26. Newman, J. C. *et al.* Ketogenic Diet Reduces Midlife Mortality and Improves Memory in
581 Aging Mice. *Cell Metabolism* **26**, 547-557.e8 (2017).

582 27. Dmitrieva-Posocco, O. *et al.* β-Hydroxybutyrate suppresses colorectal cancer. *Nature* **605**,
583 160–165 (2022).

584 28. Hopkins, B. D. *et al.* Suppression of insulin feedback enhances the efficacy of PI3K
585 inhibitors. *Nature* **560**, 499–503 (2018).

586 29. Xia, S. *et al.* Prevention of Dietary-Fat-Fueled Ketogenesis Attenuates BRAF V600E Tumor
587 Growth. *Cell Metabolism* **25**, 358–373 (2017).

588 30. Lien, E. C. *et al.* Low glycaemic diets alter lipid metabolism to influence tumour growth.
589 *Nature* **599**, 302–307 (2021).

590 31. Galiatsatos, P. & Foulkes, W. D. Familial Adenomatous Polyposis. *Am. J. Gastroenterol.*
591 **101**, 385–398 (2006).

592 32. Puchalska, P. & Crawford, P. A. Multi-dimensional Roles of Ketone Bodies in Fuel
593 Metabolism, Signaling, and Therapeutics. *Cell Metabolism* **25**, 262–284 (2017).

594 33. Nugent, K. P., Spigelman, A. D. & Phillips, R. K. S. Life expectancy after colectomy and
595 ileorectal anastomosis for familial adenomatous polyposis. *Dis. Colon Rectum* **36**, 1059–1062
596 (1993).

597 34. Jagelman, D. G., Decosse, J. J., Bussey, H. J. R. & GROUP, T. L. C. P. UPPER
598 GASTROINTESTINAL CANCER IN FAMILIAL ADENOMATOUS POLYPOSIS. *Lancet* **331**,
599 1149–1151 (1988).

600 35. Groves, C. J., Saunders, B. P., Spigelman, A. D. & Phillips, R. K. S. Duodenal cancer in
601 patients with familial adenomatous polyposis (FAP): results of a 10 year prospective study. *Gut*
602 **50**, 636 (2002).

603 36. Weiss, J. M. *et al.* NCCN Guidelines® Insights: Genetic/Familial High-Risk Assessment:
604 Colorectal, Version 1.2021. *J. Natl. Compr. Cancer Netw. : JNCCN* **19**, 1122–1132 (2021).

605 37. Karstensen, J. G. *et al.* Cancer in Patients With Familial Adenomatous Polyposis:
606 A Nationwide Danish Cohort Study With Matched Controls. *Gastroenterology* **165**, 573-581.e3
607 (2023).

608 38. Taylor, S. R., Falcone, J. N., Cantley, L. C. & Goncalves, M. D. Developing dietary
609 interventions as therapy for cancer. *Nat. Rev. Cancer* **22**, 452–466 (2022).

610 39. Goto, N. *et al.* Lymphatics and fibroblasts support intestinal stem cells in homeostasis and
611 injury. *Cell Stem Cell* **29**, 1246-1261.e6 (2022).

612 40. Crawford, P. A. *et al.* Regulation of myocardial ketone body metabolism by the gut
613 microbiota during nutrient deprivation. *Proceedings of the National Academy of Sciences of the*
614 *United States of America* **106**, 11276–11281 (2009).

615 41. Colnot, S. *et al.* Colorectal cancers in a new mouse model of familial adenomatous
616 polyposis: influence of genetic and environmental modifiers. *Lab. Investig.* **84**, 1619–1630
617 (2004).

618 42. Marjou, F. E. *et al.* Tissue-specific and inducible Cre-mediated recombination in the gut
619 epithelium. *genesis* **39**, 186–193 (2004).

620 43. Horton, J. L. *et al.* The failing heart utilizes 3-hydroxybutyrate as a metabolic stress defense.
621 *JCI insight* **4**, (2019).

622 44. Cotter, D. G., Schugar, R. C., Wentz, A. E., D'Avignon, D. A. & Crawford, P. A. Successful
623 adaptation to ketosis by mice with tissue-specific deficiency of ketone body oxidation. *American*
624 *journal of physiology. Endocrinology and metabolism* **304**, E363-74 (2013).

625 45. Schoors, S. *et al.* Fatty acid carbon is essential for dNTP synthesis in endothelial cells.
626 *Nature* **520**, 192–197 (2015).

627 46. Hsieh, W.-Y., Williams, K. J., Su, B. & Bensinger, S. J. Profiling of mouse macrophage
628 lipidome using direct infusion shotgun mass spectrometry. *STAR Protoc.* **2**, 100235 (2021).

629 47. Su, B. *et al.* A DMS Shotgun Lipidomics Workflow Application to Facilitate High-Throughput,
630 Comprehensive Lipidomics. *J. Am. Soc. Mass Spectrom.* **32**, 2655–2663 (2021).

631 48. Korotkevich, G. *et al.* Fast gene set enrichment analysis. *bioRxiv* 060012 (2021)
632 doi:10.1101/060012.

633 49. Müller-Dott, S. *et al.* Expanding the coverage of regulons from high-confidence prior
634 knowledge for accurate estimation of transcription factor activities. *Nucleic Acids Res.* **51**,
635 10934–10949 (2023).

636

637

638

639 **Table 1**

Class Description	Ingredient	D12450J	D06040601
Protein	*Casein, Lactic, 30 Mesh*	200.00g	151.00g
Protein	*Cystine, L*	3.00g	1.50g
Carbohydrate	*Starch, Corn*	506.20g	40.00g
Carbohydrate	*Lodex 10*	125.00g	0.00g
Carbohydrate	*Sucrose, Fine Granulated*	72.80g	4.00g
Fiber	*Solka Floc, FCC200*	50.00g	50.00g
Fat	*Soybean Oil, USP*	25.00g	25.00g
Fat	*Lard*	20.00g	336.00g
Mineral	*S10026B*	50.00g	50.00g
Vitamin	*Choline Bitartrate*	2.00g	2.00g
Vitamin	*V10001C*	1.00g	1.00g
Dye	*Dye, Yellow FD&C #5, Alum. Lake 35-42%*	0.04g	0.03g
Dye	*Dye, Blue FD&C #1, Alum. Lake 35-42%*	0.01g	0.03g
		1055.05g	660.55g

640

641 ***Figure 1. Ketogenic diet enhances intestinal stem cell activity and promotes***
642 ***tumorigenesis***
643 (a) Schematic of experimental design utilizing ketogenic diet (KD) in Lgr5-2A-EGFP-2A-
644 CreERT2 mice.
645 (b) Body weight of control diet (CD) and KD-fed mice over the study period.
646 (c) Circulating β-hydroxybutyrate (BHB) levels in KD-fed mice compared to CD-fed controls.
647 (d) Blood glucose levels in CD- and KD-fed mice.
648 (e) Circulating insulin levels in KD-fed mice relative to CD-fed mice.
649 (f) Representative immunohistochemistry images of Lgr5-GFP+ crypt base cells and BrdU+
650 cells in CD- and KD-fed mice.
651 (g) Quantification of BrdU+ proliferative cells in the intestinal crypt.
652 (h) Representative images and (i) quantification of *in vitro* organoid-forming assays from crypts
653 isolated from CD- and KD-exposed mice.
654 (j) Intestinal tissue BHB levels in CD- and KD-fed mice.
655 (k) Schematic of tumorigenesis protocol using Vil-CreERT2;Apc$^{fl/wt}$ mice following tamoxifen
656 induction and dietary randomization.
657 (l) Kaplan-Meier survival curves with log-rank Mantel-Cox test comparing CD- and KD-fed
658 cohorts.
659 (m) Representative images and (n) quantification of tumour burden in KD-fed mice relative to
660 CD-fed mice.
661 (o) Immunofluorescence of nuclear β-catenin, HCAR2 and DAPI in early adenomas.
662 Data are mean ± s.d.
663

664 ***Extended Data Figure 1. Metabolic and histological alterations in intestinal tissue***
665 ***following ketogenic diet exposure.***
666 (a) Composition of the 80% lard-based ketogenic diet (KD).
667 (b-c) Detailed body weight measurements of CD- and KD-fed male and female mice across the
668 experimental timeline.
669 (d) Representative image and (e) quantification of Paneth cell numbers in crypts of CD- and KD-
670 fed mice.
671 (f) Representative sorting plot of Lgr5-IRES-EGFP-CreERT2 mice fed CD or KD and (g)
672 corresponding quantification of Paneth, GFP-hi, and GFP-lo populations.
673 (h) *In vitro* clonogenicity of GFP+ ISCs isolated from CD- and KD-fed mice.
674 (i) Immunoblot of isolated crypts from CD- and KD-fed mice probed for HMGCS2, CPT1a,
675 BDH1, OXCT1, and vinculin as a loading control.
676 (j) Correlation analyses between tumour burden and serum ketone levels and (k) serum glucose
677 at the time of sacrifice.
678 (l) cartoon schematic of 90 day Apc-het model
679 (m) Tumour burden in KD- and CD-fed mid with (n) representative H&E images.
680 Data are mean ± s.d.
681

682 ***Extended Data Figure 2. HCAR2 expression in intestinal tissues and early adenomas.***
683 (a) Representative immunohistochemistry staining for HCAR2 in early intestinal adenomas in
684 CD- and KD-fed mice.
685 (b) Immunofluorescent co-stianing for β-catenin and HCAR2 around early adenomas in CD- and
686 KD-fed mice.
687 (c) UMAP of mouse intestine populations from Aliluev dataset
688 (d) Gene expression of Hcar2 in characterized cell populations annotated in Aliluev dataset with
689 corresponding marker gene dotplot visualization and number of detected genes (f) and UMIs (g)
690 split by cell type.
691 Data are mean ± s.d.
692
693

694 ***Figure 2. Loss of epithelial or systemic ketogenesis does not mitigate the pro-***
695 ***tumorigenic effects of a ketogenic diet.***
696 (a) UMAP visualization of 15,053 single cells isolated from the intestinal epithelium of control
697 diet (CD) and ketogenic diet (KD) mice, colored by cell type.
698 (b) Differential gene expression of ISCs from KD- and CD-fed mice
699 (c) Hmgcs2 expression in ISCs from CD and KD mice.
700 (d,e) Schematic of beta-oxidation and ketogenesis with inducible Hmgcs2 knockout (iKO)
701 models
702 (f) Confirmation of Hmgcs2 deletion in the intestinal epithelium of iKO mice by
703 immunohistochemistry.
704 (g) Quantification of beta-hydroxybutyrate (BHB) levels in intestinal tissue of KD-fed WT and
705 iKO mice.
706 (h) Schematic of hepatocyte-specific Hmgcs2 knockout (LiKO) mice.
707 (i) Immunohistochemistry for HMGCS2 demonstrating hepatocyte-specific loss of HMGCS2
708 expression in LiKO mice.
709 (j) Serum ketone levels under KD conditions in LiKO and control mice.
710 (k) Breeding scheme to generate WT, iKO, and LiKO mice for tumorigenesis studies.
711 (l) Quantification of tumour number and tumour burden across CD and KD conditions in wild-
712 type, iKO, and LiKO mice with (m) representative H&E images.
713 Data are mean ± s.d.
714

715 ***Extended Data Figure 3. Characterization of ketogenesis and ketolysis knockout models.***
716 (a) Quality control metrics for scRNAseq datasets with marker gene dotplot visualization.
717 (b) Lipidomic profiling of intestinal tissue upon epithelial Hmgcs2 deletion under KD conditions.
718 (c) Characterization of LiKO mouse (d) weights, (e) serum glucose, and (f) serum insulin.
719
720 Data are mean ± s.d.
721

722 ***Extended Data Figure 4. Characterization of ketogenesis and ketolysis knockout models.***
723 (a) Immunoblot and (b-c) immunohistochemistry validation of BDH1 iKO and OXCT1 iKO
724 cohorts.
725 (d) Breeding strategy for tumor cohorts
726 (e) Tumour burden quantification for BDH1 iKO and OXCT1 iKO with (f) representative H&E
727 images.
728 Data are mean ± s.d.
729

730 ***Figure 3 | Tissue-specific Hmgcs2 overexpression elevates intestinal ketone body levels***
731 ***without affecting spontaneous tumorigenesis.***
732 (a) Schematic of the Rosa26-CAG-Hmgcs2-2A-mCherry-LSL (HMGCS2 iOE) mouse
733 (b) Representative immunofluorescence images showing expression of HMGCS2 and mCherry
734 throughout the intestinal epithelium following Vil-CreERT2-mediated induction.
735 (c) Quantification of β-hydroxybutyrate (BHB) levels in intestinal tissue lysates from control diet-
736 fed HMGCS2 iOE mice and WT controls.
737 (d) Breeding scheme to generate mice for tumorigenesis studies with or without concurrent
738 Hmgcs2 overexpression maintained on control diet.
739 (e) Tumour burden quantification for WT and iOE mice.
740 (f) Representative images of tumour burden along the intestinal tract.
741 Data are mean ± s.d.
742
743

744 ***Extended Data Figure 5 | Characterization of intestinal HMGCS2 overexpression and its***
745 ***impact on epithelial clonogenicity.***
746 (a) Diagram for Rosa26 targeting and Hmgcs2 iOE construct
747 (b) Immunoblot of iOE organoids treated with 4-hydroxytamoxifen in vitro
748 (c) Lipidomics of WT and iOE small intestine
749 Data are mean ± s.d.

750 ***Figure 4. Ketogenic diet enhances PPAR signaling, fatty acid oxidation gene expression,***
751 ***and ISC function via CPT1a activity.***
752 (a) Transcription factor activity inference for ISCs in CD- and KD-fed mice
753 (b) Gene set enrichment analysis (GSEA) of most increased pathways in ISCs isolated from
754 KD- and CD-fed mice
755 (c-e) PPAR signature scoring for CD- and KD- ISCs
756 (f) Cpt1a expression in CD- and KD- ISCs
757 (g,h) Schematic of beta-oxidation and ketogenesis with inducible CPT1a knockout models
758 (i) Representative H&E images with (j) quantification of total tumour number in WT and CPT1a
759 iKO mice.
760 Data are mean ± s.d.
761

762 ***Extended Data Figure 6. Augmented fatty acid oxidation signature and mechanistic***
763 ***consequences of Cpt1a deletion in KD-exposed intestinal stem cells.***
764 (a) Gene set enrichment analysis (GSEA) of most decreased pathways in ISCs isolated from
765 KD- and CD-fed mice
766 (b) Breeding schematic for inducible CPT1a knockout tumorigenesis models
767 (c) Quantification of tumour burden in WT and CPT1a iKO mice on CD.
768 (d) Representative H&E images.
769 Data are mean ± s.d.
770
771

772 ***Extended Data Figure 7. KD and ketone bodies exhibit differential effects in the colon.***
773 (a) Quantification of β-hydroxybutyrate (BHB) levels in proximal colon (pCO) and distal colon
774 (dCO) tissue lysates from conventionally housed and germ-free mice.
775 (b) Quantification of β-hydroxybutyrate (BHB) levels in proximal colon (pCO) and distal colon
776 (dCO) tissue lysates from CD and KD fed mice.
777 (c) Immunoblot of snap frozen pCO and dCO from WT, HMGCS2 iKO and HMGCS2 iOE mice
778 probed for HMGCS2 and vinculin as a loading control.
779 (d) Quantification of β-hydroxybutyrate (BHB) levels in proximal colon (pCO) and distal colon
780 (dCO) tissue lysates from WT and HMGCS2 iOE mice.
781 (e) Quantification of total tumour number from colons of CD, KD and HMGCS2 iOE (on CD)
782 mice.
783 (f) Representative H&E images corresponding to (e)
784 (g) Representative immunohistochemistry staining for HCAR2 in colon adenomas in CD- and
785 KD-fed mice.
786 Data are mean ± s.d.
787

Figure 1

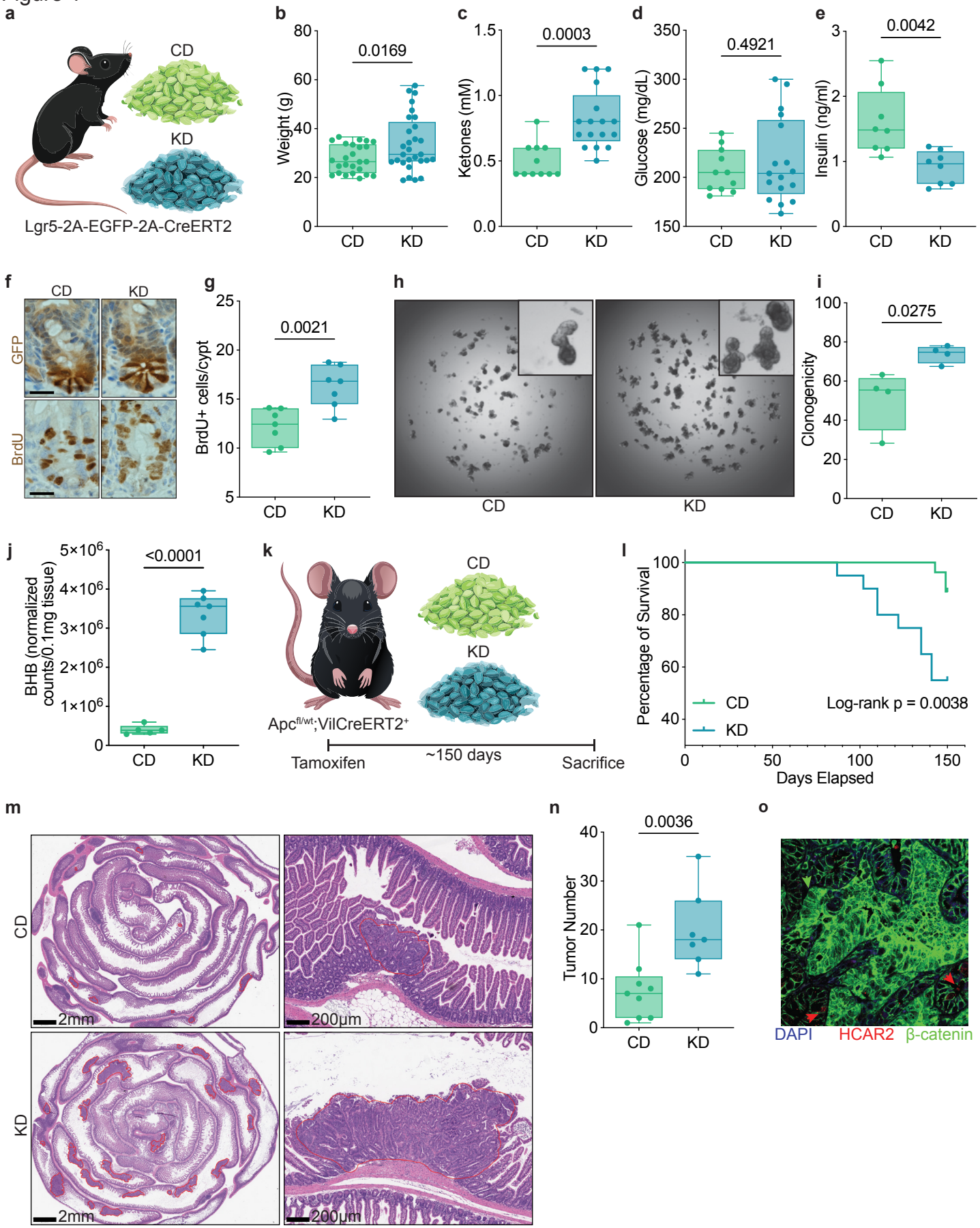
a
CD
KD
Lgr5-2A-EGFP-2A-CreERT2
b
0.0169
Weight (g)
CD
KD
c
0.0003
Ketones (mM)
d
0.4921
Glucose (mg/dL)
e
0.0042
Insulin (ng/ml)
f
GFP
BrdU
g
0.0021
BrdU+ cells/cypt
h
i
0.0275
Clonogenicity
j
<0.0001
BHB (normalized counts/0.1mg tissue)
k
Apc$^{fl/wt}$;VilCreERT2^{+}
Tamoxifen
~150 days
Sacrifice
l
Percentage of Survival
Log-rank p = 0.0038
Days Elapsed
m
2mm
200μm
n
0.0036
Tumor Number
o
DAPI
HCAR2
β-catenin

Figure 2

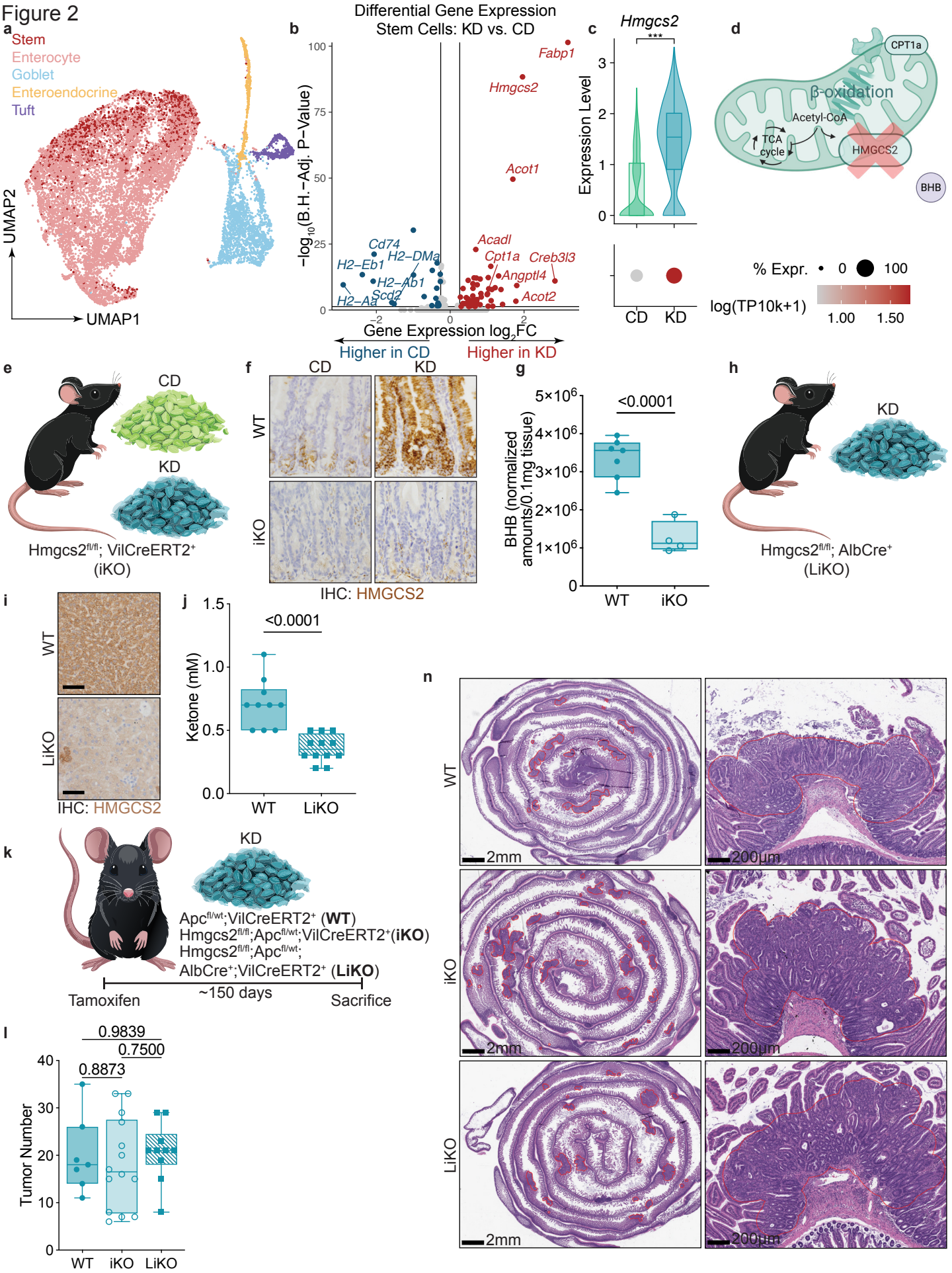
a
Stem
Enterocyte
Goblet
Enteroendocrine
Tuft
UMAP2
UMAP1
b
Differential Gene Expression
Stem Cells: KD vs. CD
−log10(B.H.−Adj. P−Value)
Fabp1
Hmgcs2
Acot1
Acadl
Cpt1a
Creb3l3
Angptl4
Acot2
Cd74
H2−DMa
H2−Eb1
H2−Ab1
Scd2
H2−Aa
Gene Expression log2FC
Higher in CD
Higher in KD
c
Hmgcs2
***
Expression Level
CD
KD
d
CPT1a
β-oxidation
Acetyl-CoA
TCA cycle
HMGCS2
BHB
% Expr.
0
100
log(TP10k+1)
1.00
1.50
e
CD
KD
Hmgcs2fl/fl; VilCreERT2+
(iKO)
f
CD
KD
WT
iKO
IHC: HMGCS2
g
<0.0001
BHB (normalized amounts/0.1mg tissue)
WT
iKO
h
KD
Hmgcs2fl/fl; AlbCre+
(LiKO)
i
WT
LiKO
IHC: HMGCS2
j
<0.0001
Ketone (mM)
WT
LiKO
k
KD
Apcfl/wt;VilCreERT2+ (WT)
Hmgcs2fl/fl;Apcfl/wt;VilCreERT2+(iKO)
Hmgcs2fl/fl;Apcfl/wt;
AlbCre+;VilCreERT2+ (LiKO)
Tamoxifen
~150 days
Sacrifice
l
0.9839
0.7500
0.8873
Tumor Number
WT
iKO
LiKO
n
WT
iKO
LiKO
2mm
200μm

Figure 3

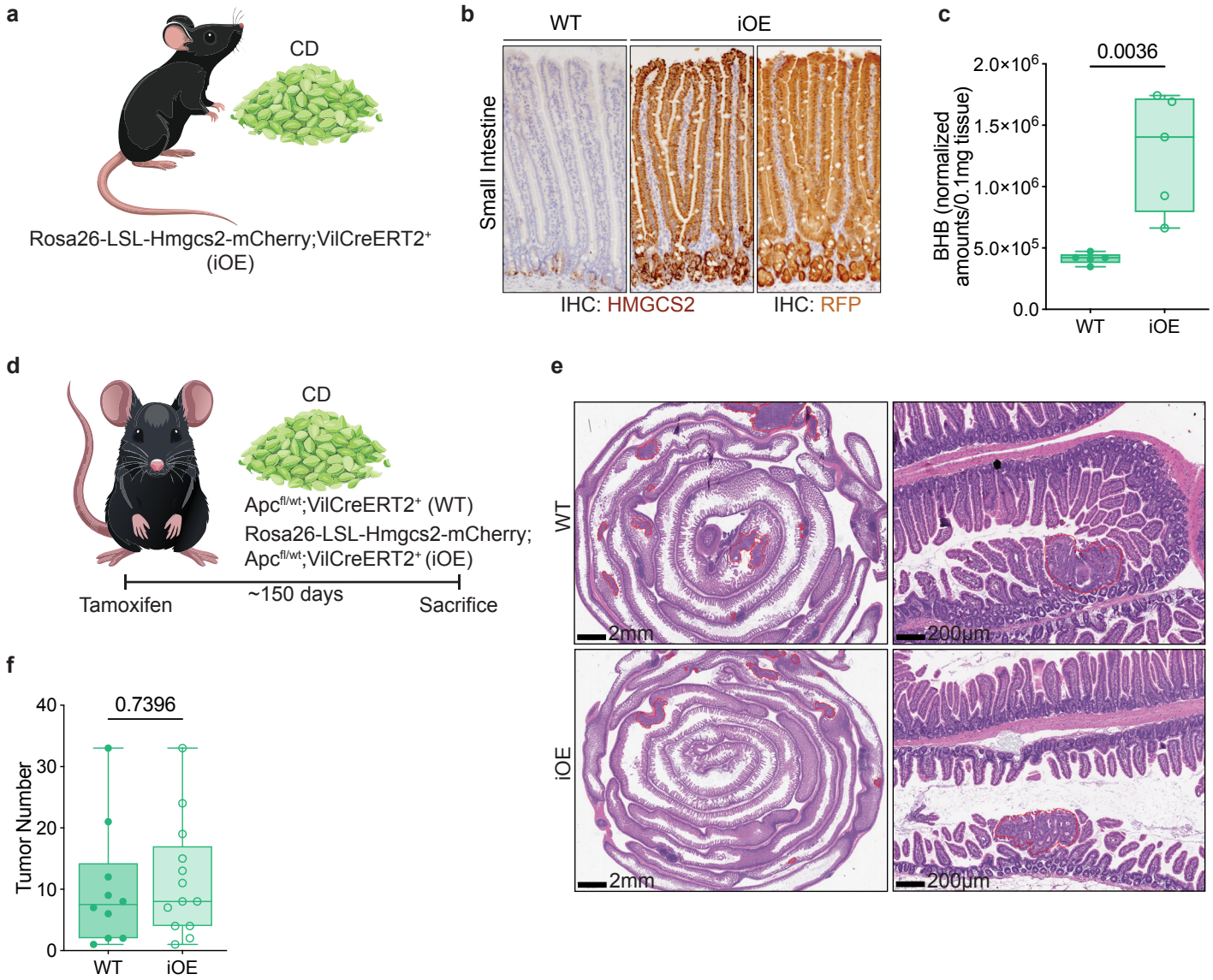
a
CD
Rosa26-LSL-Hmgcs2-mCherry;VilCreERT2+
(iOE)
b
WT
iOE
Small Intestine
IHC: HMGCS2
IHC: RFP
c
0.0036
BHB (normalized amounts/0.1mg tissue)
2.0×10^6
1.5×10^6
1.0×10^6
5.0×10^5
0.0
WT
iOE
d
CD
Apc^fl/wt;VilCreERT2+ (WT)
Rosa26-LSL-Hmgcs2-mCherry;
Apc^fl/wt;VilCreERT2+ (iOE)
Tamoxifen
~150 days
Sacrifice
e
WT
iOE
2mm
200μm
f
0.7396
Tumor Number
40
30
20
10
0
WT
iOE

Figure 4

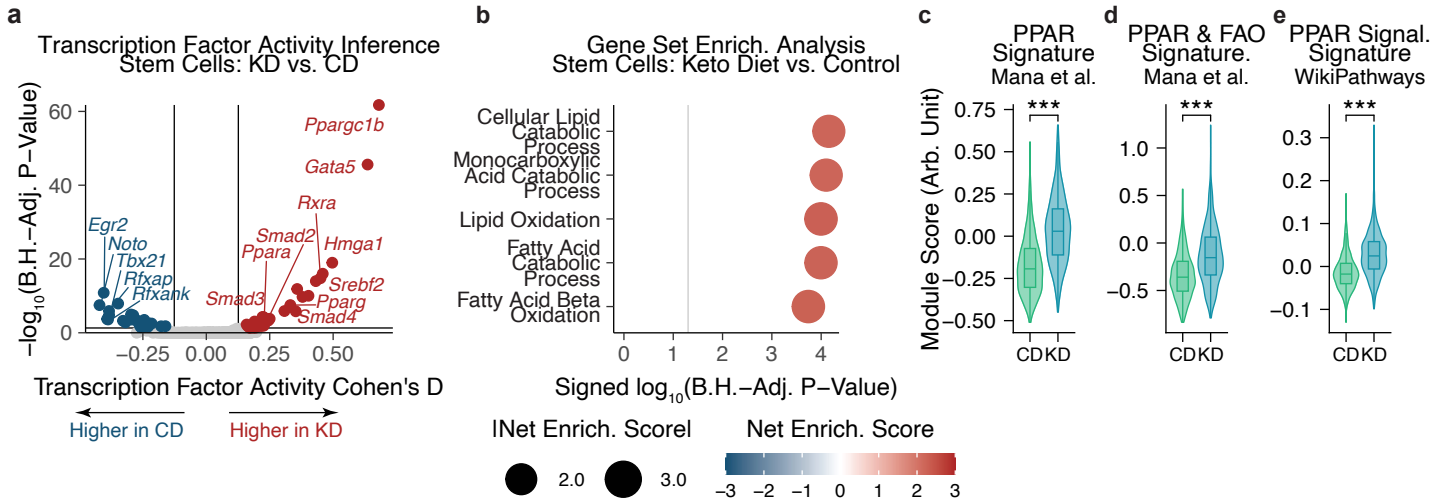
a
Transcription Factor Activity Inference
Stem Cells: KD vs. CD
−log10(B.H.−Adj. P−Value)
Ppargc1b
Gata5
Rxra
Egr2
Noto
Tbx21
Rfxap
Rfxank
Smad2
Ppara
Hmga1
Smad3
Srebf2
Pparg
Smad4
Transcription Factor Activity Cohen's D
Higher in CD
Higher in KD
b
Gene Set Enrich. Analysis
Stem Cells: Keto Diet vs. Control
Cellular Lipid Catabolic Process
Monocarboxylic Acid Catabolic Process
Lipid Oxidation
Fatty Acid Catabolic Process
Fatty Acid Beta Oxidation
Signed log10(B.H.−Adj. P−Value)
INet Enrich. Scorel
Net Enrich. Score
c
PPAR Signature
Mana et al.
Module Score (Arb. Unit)
d
PPAR & FAO Signature.
Mana et al.
e
PPAR Signal. Signature
WikiPathways
CD KD

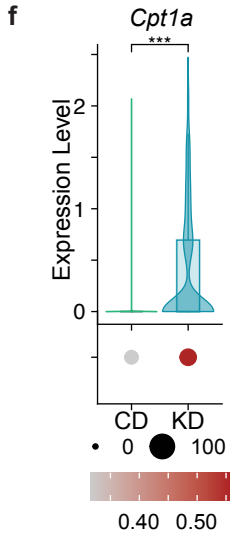
f
Cpt1a
Expression Level
CD KD

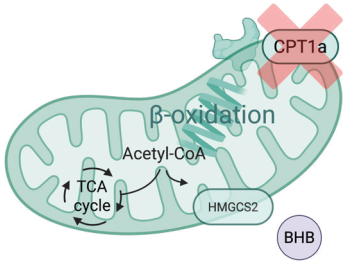
g
CPT1a
β-oxidation
Acetyl-CoA
TCA cycle
HMGCS2
BHB

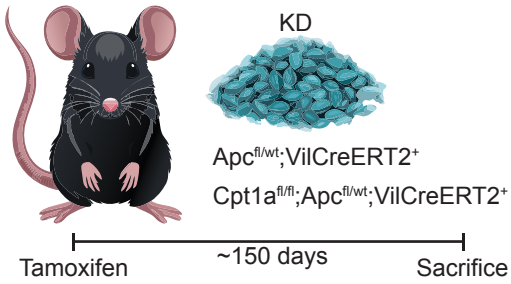
h
KD
Apc fl/wt;VilCreERT2+
Cpt1a fl/fl;Apc fl/wt;VilCreERT2+
Tamoxifen
~150 days
Sacrifice

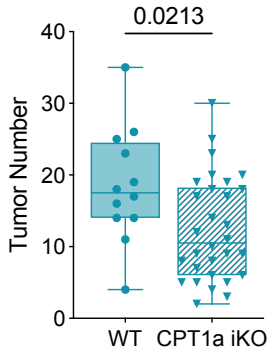
i
0.0213
Tumor Number
WT
CPT1a iKO

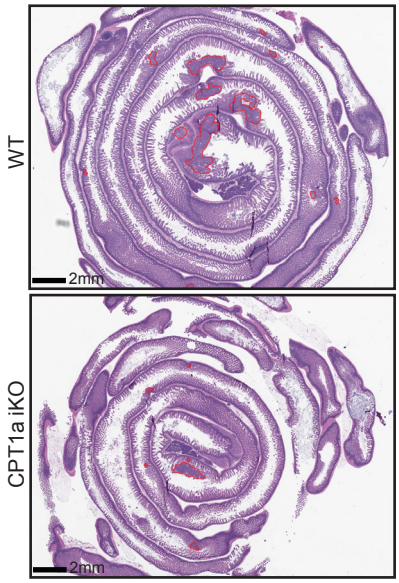
j
WT
CPT1a iKO
2mm